JOURNAL OF MATERIALS SCIENCE 28 (1993) 4821–4828

Fabrication of engineering ceramics by injection moulding a suspension with optimum powder properties

Part II *Mechanical properties and wear behaviour*

R. E. F. Q. NOGUEIRA, D. T. GAWNE, M. J. EDIRISINGHE*
Department of Materials Technology, Brunel University, Uxbridge, Middlesex UB8 3PH, UK

The mechanical properties of alumina test bars fabricated using injection moulding as the shaping operation, are described. The modulus of rupture, hardness, fracture toughness and wear behaviour of the ceramic specimens are reported. Test bars were injection moulded using a polypropylene-based high molecular weight organic vehicle. The processing and microstructure of the test bars were discussed in Part I. The alumina powder was selected in a previous investigation, which considered the compounding, compression moulding, removal of organic vehicle and sintering of several formulations containing different alumina powders.

1. Introduction

The increase in the demand for engineering ceramics in recent years has generated a great deal of interest in the mechanical properties of these materials. The high melting point of ceramics dictates that artefacts have to be fabricated by assembling powder particles to the required shape. The characteristics of ceramic powders, e.g. size distribution and shape, are also important, but once the ceramic powder has been selected (e.g. this investigation) the fabrication process used has a significant influence on the microstructure and properties of the ceramic [1, 2]. Many processes, such as pressing, extrusion, slip casting and injection moulding, are available for fabrication of ceramic shapes and all these require a final sintering stage in order to achieve a high density. Defects are mainly introduced at the fabrication stage and once this happens they are retained as strength-limiting flaws in ceramic artefacts. Therefore, it is important to assess the properties of the ceramic bodies in relation to the fabrication procedure used.

The strength of ceramic materials is generally characterized by flexure testing, also referred to as bend testing [3–5]. A flexural strength test is based on simple bending theory and consists of a bar of the material supported at two ends and loaded from above at one (three-point bend test) or two (four-point bend test) points. The outermost fibres of a bend specimen experience uniaxial tensile stress. Bend strength is defined as the maximum value of this tensile stress (at failure) and is often called the modulus of rupture (MOR). For a rectangular specimen such as the sintered test bars used in this investigation

$$\text{MOR} = \frac{3Fl}{2bd^3} \quad (1)$$

where F is the load at failure and l is the load span, b and d are the width and thickness of each specimen, respectively.

Strength values of ceramics show wide scatter and are therefore analysed statistically, the most common method being Weibull statistics [4, 6, 7]. Thus, the equation

$$\frac{1}{1-P} = \exp(\sigma/\sigma_0)^m \quad (2)$$

is usually used to analyse statistically strength values obtained from testing of ceramics. P is the probability of failure at the stress, σ, and can be calculated using a standard procedure (e.g. [8–10]). m and σ_0 are constants; m is defined as the Weibull modulus, which is an estimate of the reliability of the component, and is obtained by calculating the gradient of the graph of the logarithmic form of Equation 2.

There is a lack of standards for the hardness testing of ceramic materials. However, macro-indentation methods, such as the Vickers hardness test, have been widely applied to investigate the hardness of ceramic materials [11–13]. Micro-hardness tests are not favoured for measuring the hardness of high-alumina ceramics due to inconsistency of results [11, 13]. Hardness values of ceramic materials show considerable scatter mainly due to the presence of defects such as cracks and porosity [13] and therefore it is recommended that 5–10 randomly positioned indentations are made to estimate the macrohardness of a ceramic [14].

* Author to whom all correspondence should be addressed.

0022–2461

In the absence of a standard test, indentation methods have been widely used to evaluate the fracture toughness of ceramics [12, 15–17]. In one such method, the indentation causes cracks and the measurement of crack lengths leads to an estimate of the fracture toughness (DCM method). On the other hand, fracture toughness can be estimated from strength measurements such as in the single-edge notched beam (SENB) method. The DCM method is simpler and requires small specimens which must be carefully prepared so that they are free of surface stresses prior to indentation. However, post-indentation slow crack growth is a problem [18]. Also, there is no accepted formula to calculate the fracture toughness, K_{IC}, from results of this test and the method tends to overestimate the fracture toughness. In fact, over a dozen expressions are found in the literature [15, 19]. Liang *et al.* [17] have proposed the equation

$$(K_{IC}\phi/H_V a^{1/2})\,(H_V/E\phi)^{0.4}\,\alpha = (c/a)^{(c/18a)-1.51} \quad (3)$$

where H_V is the Vickers hardness, $2a$ is the length of the diagonal of the square indentation produced by the Vickers hardness test, E is the Young's modulus, and $2c$ is the crack length. ϕ is a constraint factor (~ 3) and α is given by the expression.

$$\alpha = 14\{1 - 8[(4\nu - 0.5)/(1 + \nu)]^4\} \quad (4)$$

where ν is the Poisson's ratio of the material. K_{IC} values obtained by the DCM method and Equation 3 compared with those determined using the SENB method did not show a significant difference for alumina ceramics having grain sizes in the range 2–12 μm up to indentation loads of 300 N [17].

Because ceramic materials have a high hardness, they are frequently used in engineering applications where adverse tribological conditions persist and therefore the assessment of their resistance to wear is extremely important. However, wear resistance is not an intrinsic property of the material but is related to the engineering system in which the material is used [20, 21]. Current understanding of wear of ceramics is inadequate for predicting reliable data for design purposes [22–25].

Several parameters (e.g. microstructural features, test procedure and surrounding atmosphere) affect wear test results of ceramics [26–28]. Therefore, to date, there is no universal sliding wear test and only a few devices are standardized [29]. The reciprocating pin-on-flat wear test used with a diamond indentor in this investigation is useful to simulate sliding wear of the heavy abrasive type [30]. There are three main methods by which wear can be measured [29]; by weight loss of specimens, by weighing the wear debris produced, or by following the dimensional changes which occur as a result of wear (e.g. wear scar depth). The last method was used in the present work.

In this investigation the flexure strength, hardness, fracture toughness and wear behaviour of a well-characterized batch of alumina specimens have been determined. These specimens have been fabricated using an injection moulding processing route. An extensive data review [31] published by the National Physical Laboratory (NPL) UK, which classifies high-alumina ceramics into groups (A1–A12) according to the aluminium oxide content, and analyses their structure and properties, provides a basis for the comparison of the properties of these specimens with those made using other commercially available aluminas. Also, mechanical properties of injection moulded ceramics are scarce in the literature and this investigation allows the comparison of the properties measured with those obtained for alumina specimens made using similar and other processing methods.

2. Experimental procedure

2.1. Materials and processing

A152.SG (Alcoa Manufacturing (GB), Worcester, UK) was the alumina ceramic powder used. Particle characteristics of this powder have been described in Part I [32]. The test bars were made by injection moulding a suspension containing 63 vol % alumina powder dispersed in a polypropylene-based organic vehicle. Twin-screw extrusion was used to disperse the ceramic powder in the organic vehicle. The injection moulded test bars were subjected to slow pyrolysis in static air to remove the organic vehicle. Test bars were subsequently sintered by heating in static air to 1650 °C at 30 °C min^{-1} and soaking at this temperature for 2 h followed by cooling in the furnace to room temperature. Full details of the organic vehicle used and processing are given in Part I [32].

2.2. Flexural strength testing

A standard jig fitted to a model 4206 Instron universal testing machine was used to test 30 sintered bars in three-point bending. The testing conditions are given in Table I. The load span was limited to 39 mm due to the geometries of the specimen and the jig. Halves of test bars resulting from flexure tests were used for hardness, fracture toughness and wear tests described below.

2.3. Hardness testing

Vickers hardness testing was used with a load of 20 kg. The specimens were degreased with an organic solvent before testing. Each specimen was subjected to at least 15 indentations.

2.4. Fracture toughness testing

The indentation method was used to determine the fracture toughness. This required the measurement of the lengths of cracks originating from the corners of Vickers hardness test impressions.

TABLE I Conditions for flexural testing

Crosshead speed (mm min^{-1})	0.5
Load span (mm)	39
Humidity (%)	50
Temperature (°C)	23

Specimens were mounted in cold resin and polished to improve reflectivity, allowing a more precise measurement of crack lengths. The polishing sequence was as follows. Initially, the specimens were ground with SiC powder on a flat glass plate. SiC powders with average particle sizes of 170, 30, 20 and 12 μm were used in the sequence given. Subsequently, the specimens were polished with 6 and 1 μm diamond pastes.

Each specimen was subjected to at least five indentations using a 40 kg load. After indentation, the crack lengths were measured. Measurements were repeated 24 h later when the cracks had stabilized. The average of the two measurements was used in the calculations. Tests were also done using soda–lime glass having a known fracture toughness to ensure the validity of the experiments.

2.5. Wear testing

Broken halves of specimens used for flexure tests, measuring approximately 30 mm × 11 mm × 3 mm, were tested under sliding wear conditions using a reciprocating pin-on-flat wear machine. Each specimen tested was fixed in the specimen holder which moved in reciprocating fashion at a selected speed. In this investigation the speed was fixed at 50 cycles per minute. A Rockwell diamond cone indentor was used as the pin, and it was pressed against the specimen under different loads, ranging from 10–60 N.

Initially, the specimens were tested as-sintered, without preparing the surface, because the surface roughness average, R_a, was ~0.6 μm. However, variations in the thicknesses of the samples, of up to 200 μm, made the results of wear tests inconsistent, particularly under lower loads. It was then decided to grind and polish the specimens by mounting them in cold resin, applying the same procedure described in Section 2.4 above. The back of the mounting was machined flat, parallel to the surface to be tested. This was done to ensure that the surface of each specimen was horizontal. After this procedure, the largest variation in height between any two points of the surface was 10 μm. Wear was measured as the depth of the track made by the indentor corresponding to a given number of cycles. This was measured by a linear voltage displacement transducer, and the signal was registered on a chart recorder. Test duration was 1 h for each track (3000 cycles), and three or four tracks were made on each specimen. Environmental conditions were not controlled, but both ambient temperature and humidity were measured before and after each test to ensure that there was no significant change in these parameters during testing.

The specimens were examined in a Talysurf 4 (Taylor Hobson, Leicester, UK), before and after being tested in order to calibrate the wear measurements.

2.6. Microscopy

Fracture surfaces of test bars resulting from flexural testing and specimens subjected to wear tests were examined using a Cambridge S250 scanning electron microscope. All specimens were lightly coated with gold to prevent charging during microscopical examination.

3. Results and discussion

3.1. Specimen characteristics

A batch of sintered alumina test bars used in this investigation is shown in Fig. 1. The linear shrinkage from the as-moulded to the sintered stage is 12.96 % (standard deviation 0.21) which corresponds to a volume shrinkage of ~38 %. As reported previously [32], these test bars have a relative density of ~96 % (standard deviation 0.6) and their average grain size is ~7 μm [32].

The Al_2O_3 content of the as-received alumina powder is 99.7 wt % (manufacturers specifications). Taking into consideration the 0.25 wt % MgO added as a sintering aid [32], these specimens fall into Group A5 of the NPL classification [31] where the Al_2O_3 content is 99–99.6 wt %.

3.2. Flexural strength

Flexural strength results (Table II) show an average value of 268 MPa (standard deviation 45). The NPL data review suggests a three-point bend average flexural strength of 200–250 MPa for an average grain size of ~7 μm [31] but the fabrication procedure of the test bars is not mentioned. Mutsuddy [33] and Fanelli *et al.* [34] report flexural strengths of 260 MPa (standard deviation 53) and 309 MPa (standard deviation 6), respectively, for alumina bodies injection moulded using A16.SG alumina.

Compared with A152.SG alumina used in this investigation, A16.SG is a powder with a narrower particle-size distribution and a smaller median particle size. Hence, better sinterability is expected [35]. However, the relative density and average grain size of the specimens quoted by Mutsuddy [33] was 97%, and 13 μm, respectively. In comparison, Fanelli *et al.* [34] used specimens with a relative density of 94%, but grain size measurements are not mentioned. To complicate matters further, Mutsuddy [33] and Fanelli *et*

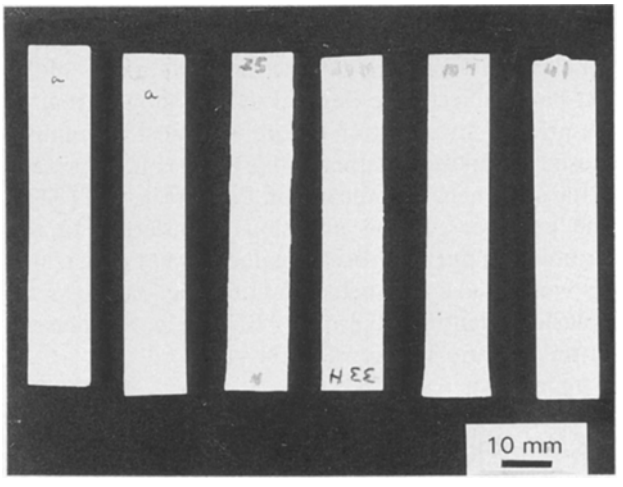

Figure 1 A batch of sintered alumina test bars used in this work.

TABLE II Flexural strength of injection moulded alumina specimens (three-point bend test)

Specimen	Flexural strength (MPa)	Specimen	Flexural strength (MPa)
1	277	16	268
2	280	17	225
3	250	18	294
4	224	19	274
5	287	20	282
6	317	21	271
7	249	22	204
8	251	23	257
9	235	24	198
10	339	25	202
11	376	26	279
12	237	27	236
13	241	28	255
14	337	29	315
15	220	30	358

al. [34] used four-point and three-point bend tests, respectively. In general, three-point bend tests report higher average strength values with greater scatter in results [36] but four-point bend testing requires stringent control of jig-specimen alignment [37] and it is difficult to ensure this, especially with brittle materials. Although the flexural strength values reported in this investigation broadly agree with the values quoted in the literature [31, 33, 34], different test procedures, relative densities and microstructures make close comparison impossible.

Fanelli *et al.* [34] also suggest that the flexural strength of injection moulded alumina ceramics is similar to that of pressed and slip-cast bodies. They also indicate that the hardness of injection moulded and slip-cast alumina is higher than that of a pressed body. It is interesting that in these comparisons the injection moulded alumina specimens had a lower density [34]. In fact, it has been suggested that, in comparison with pressing, an injection moulding processing route achieves a lower final density for a combination of alumina powder characteristics [38]. However, powder characteristics have to be optimized for each fabrication procedure and therefore the above comparison is not completely valid.

Failure of alumina at room temperature is usually caused by the propagation of an isolated defect or the linking together of several small defects [39]. Scanning electron microscopy of the fracture surfaces of the test bars subjected to flexural testing showed that in the present investigation failure was most commonly caused by linking together of fine pores (Fig. 2) present in the specimens as indicated in Part I (Fig. 9 of [32]). The presence of iron inclusions transferred to the formulation during processing due to wear of machinery would have also helped failure. Fig. 3a shows an inclusion, identified as iron by EDX (Fig. 3b), present on the fracture surface of a test bar.

3.3. Weibull modulus

The flexural strength values were plotted (Fig. 4) according to Equation 2 to determine the Weibull

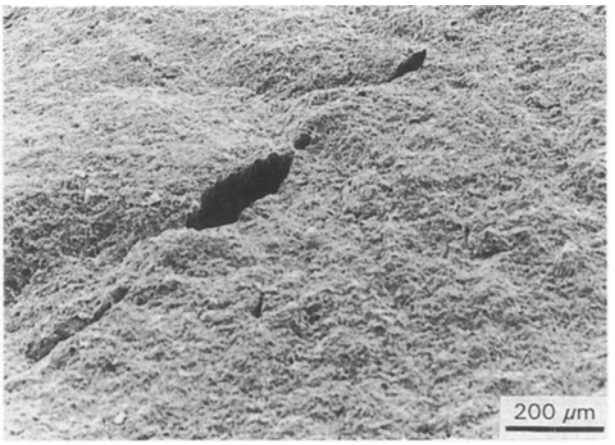

Figure 2 Scanning electron micrograph showing the linking together of fine pores to give failure in most test bars.

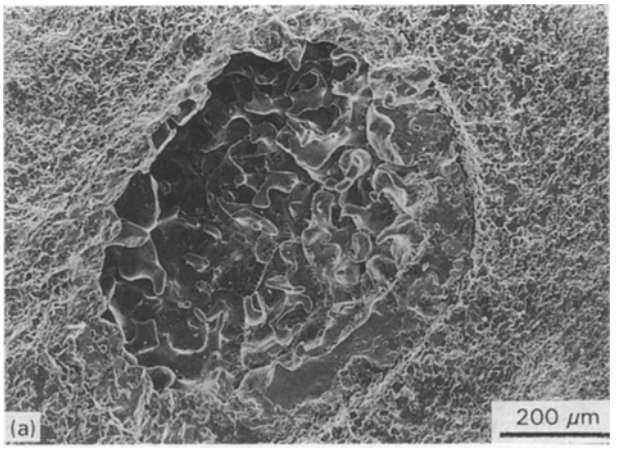

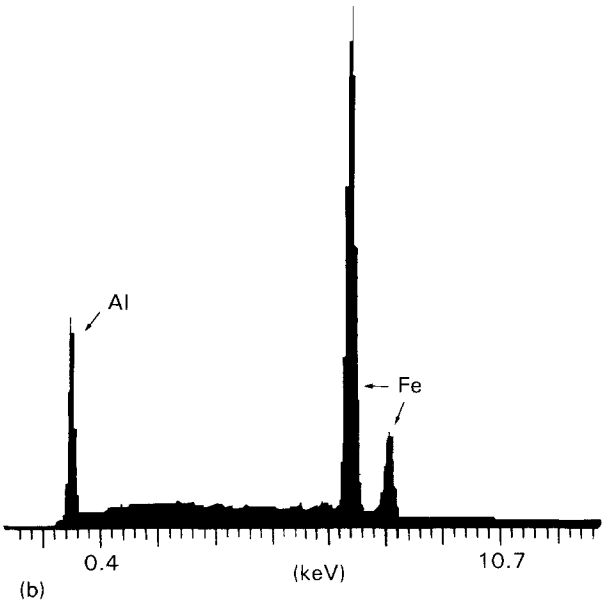

Figure 3 (a) Scanning electron micrograph showing an inclusion present on the fracture surface of a test bar. (b) EDX analysis in the region of the inclusion.

modulus, m. From Fig. 4, $m \simeq 7$ for the batch of specimens used in this investigation. Some commercial ceramic products claim to have much higher m values, in the range 15–20, but according to Boch *et al.* [40] these refer to strength tests done on small bars which have been carefully polished and prepared by cold

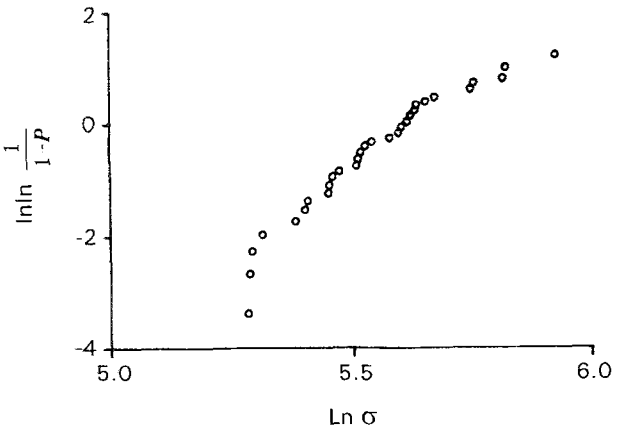

Figure 4 Logarithmic plot of Equation 2 to estimate the Weibull modulus.

isostatic pressing, whereas for actual injection moulded and coarse-ground components, m is closer to 10. In general, fine machining, polishing and smoothing of sharp edges increases the Weibull modulus of test bars compared with those subjected to testing in the as-sintered condition [41], as in this investigation.

The batch size of 30 specimens was considered to be large enough to estimate an average flexural strength and Weibull modulus. Glandus and Boch [42] investigated the influence of the number of specimens tested on the mean strength and Weibull modulus values. They concluded that the mean strength of alumina ceramics could be estimated to an acceptable accuracy using a batch of 10 specimens. In the case of the Weibull modulus, a batch of 30 specimens gave an uncertainty of approximately 13%. In a recent collaborative research programme in which seven laboratories from four countries took part [43], a sample size of 30 specimens was chosen as a compromise between obtaining narrow confidence limits and economic considerations. In fact, sintered alumina ceramics with 99.5% relative density were tested and Weibull modulus values ranging between 7 and 13 were reported [43].

3.4. Hardness

Results (Table III) show that the batch of specimens tested have an average hardness of 1540 kg mm^{-2} (standard deviation 55). The only direct comparison available in the literature [34] is 1467 kg mm^{-2} (standard deviation 91) reported for injection moulded alumina samples where the starting powder was A16.SG alumina.

In general, a higher hardness can be achieved in high alumina ceramics by increasing the alumina content [13]. A finer grain size increases the hardness, although some microhardness results have indicated the opposite trend [13]. However, per cent porosity rather than grain size is more effective in controlling hardness in high density, high-alumina ceramics [11]. The load used for indentation also affects the hardness values reported [31] with the hardness increasing with decreasing load because of the response, i.e. plastic

TABLE III Hardness values reported as the average of 15 indentations. Standard deviation of hardness values for each sample are given in parenthesis

Specimen	Hardness (kg mm^{-2})	Specimen	Hardness (kg mm^{-2})
1	1524 (90)	14	1570 (110)
5	1564 (51)	15	1460 (166)
7	1519 (164)	19	1524 (65)
8	1656 (225)	24	1564 (51)
9	1466 (163)	26	1505 (97)
11	1494 (66)	28	1506 (112)
12	1658 (178)	29	1564 (55)
13	1511 (134)	30	1566 (109)

flow, densification of porosity and fracture, of the material under the high local pressure of the indentor. The above reasons make comparison of the results obtained in this investigation with the NPL classification [31] values for group A5 alumina difficult. The closest comparison is a hardness value of 1357 (standard deviation 51) measured under a load of 10 kg for a Group A5 alumina having ~4 μm mean grain size but the fabrication route used to produce the specimens tested was not mentioned.

3.4. Fracture toughness

Results (Table IV) show that the present batch of alumina specimens tested show an average K_{IC} value of 4.1 MPa m$^{1/2}$ (standard deviation 0.3) and therefore is in the range 3.5–5.5 MPa m$^{1/2}$ expected for Group A5 high alumina ceramics [31]. However, it is lower than the value obtained by Liang *et al.* [17] who proposed Equation 3.

The Young's modulus and Poisson's ratio values used to calculate K_{IC} using Equation 3 were corrected according to the method suggested by Morrell [31] to account for the 4.3 vol % porosity present. Considering that these specimens were only ~96 % dense and the fact that they contained micro-pore type defects (as discussed in Part I), the calculated K_{IC} value of ~4 MPa m$^{1/2}$ seems high. However, K_{IC} is also dependent on grain size with a larger grain size increasing the K_{IC} value of ceramics [31, 43].

3.5. Wear behaviour

Fig. 5 shows how the penetration depth of the diamond-tipped slider increases with the number of sliding cycles for four applied loads. Two stages of wear are evident. The first stage up to approximately 500 cycles shows a high wear rate (running-in wear), which subsequently gives way to milder wear in the second stage (equilibrium wear). The average wear rate in both of these stages increases approximately linearly with the applied load (Fig. 6).

SEM observations on the worn surfaces of the alumina revealed increased surface damage with increasing load (Fig. 7). The observations also showed extensive plastic deformation, particularly in Fig. 7b, in which the alumina has been smeared into smooth flat regions with torn edges. Plastic deformation is not observed in alumina under tensile loading but is

TABLE IV Fracture toughness of alumina calculated using Equation 3

Specimen	K_{IC} (MPa $m^{1/2}$)
7	4.27
14	4.30
25	4.04
28	4.30
30	3.63

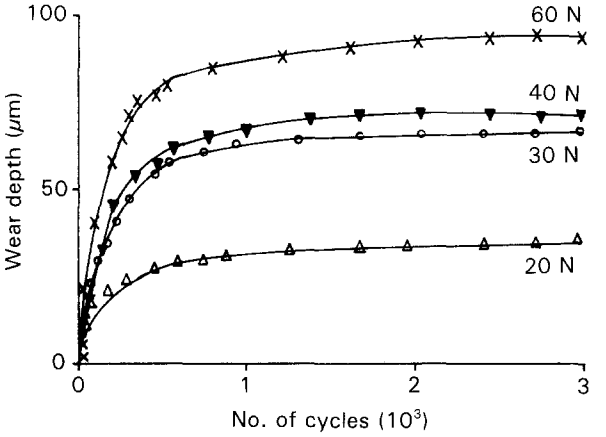

Figure 5 Wear of alumina under various loads in the reciprocating diamond scratch test.

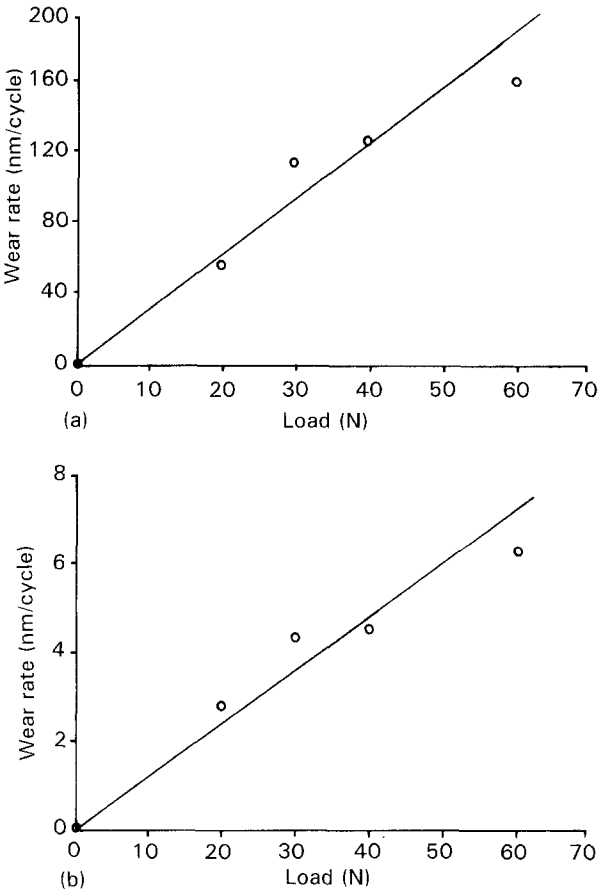

Figure 6 Wear of alumina as a function of load for (a) running-in, and (b) equilibrium wear stages.

shown to take place under the high hydrostatic compressive stresses encountered at a sliding interface [44].

In addition to the smooth deformed regions, the wear track also contains many deep pits (Fig. 7). These pits could be the valleys in the initial topography in which only the peaks were deformed. In order to check this possibility, the R_a value of the alumina surface before wear was measured and the R_t value estimated. The R_a value represents the average peak height, whereas the R_t value, more usefully in this case, gives the difference in height between the highest peak and the deepest valley. Previous work on alumina [45] showed that $R_t \simeq 7\,R_a$, so that for the measured R_a value of 0.6 μm, R_t is estimated at 4 μm. Wear depths of up to 100 μm were measured in the current experiments and so it is concluded that the pits observed (Fig. 7) are not due to the valleys in the initial surface topography.

Close examination of Fig. 7c shows the presence of fine cracks and pits of a similar size to that of the constituent grains. The cracks appear to delineate regions corresponding to the alumina grains. The following mechanism for material removal from the surface appears likely.

Plastic deformation takes place leading to dislocation pile-ups and crack initiation at grain boundaries oriented at right angles to the sliding direction at the surface due to the high tensile stresses generated by the frictional forces during sliding. The cracks initially extend along the grain boundaries in the traverse direction owing to their relatively low fracture toughness, and then follow the grain contours until eventually the entire grain is circumvented and plucked out of the surface to form a pit. The wear debris (Fig. 8) contains many particles much smaller than the grain size, which is most likely because the pulled-out grains are comminuted between the sliding surfaces.

The wear rates in the running-in stage were approximately 25 times those in the equilibrium stage. This ratio is generally much higher than those encountered for metals, for which values of 5–10 times are more common [46]. The particularly high wear rates of alumina in the running-in period are attributed to its low fracture toughness (compared with metals) and the roughness of the initial surface, in which the exposed peaks experience tensile stresses and consequently suffer fast fracture on contact with the sliding counterface. The sensitivity of the wear of ceramics to the initial surface roughness has been demonstrated previously [44]. After the removal of these high spots, the remaining surface topography is sufficiently constrained by the surrounding material to enable hydrostatic compressive stresses to be developed with the accompanying plastic deformation and reduced wear rates. The scale of fracture therefore shifts from macroscopic during running-in, to microscopic in the equilibrium stage.

Wear of alumina during the running-in stage follows a brittle fracture mechanism with rapid material-removal rates, whereas in the equilibrium stage, plastic deformation is prevalent and the wear behaviour tends somewhat to be similar to that of metals. The initial surface finish of alumina is therefore critical and a smooth surface will clearly be beneficial in

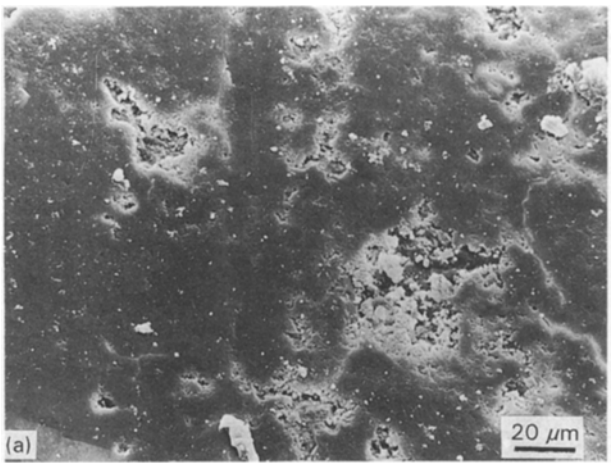

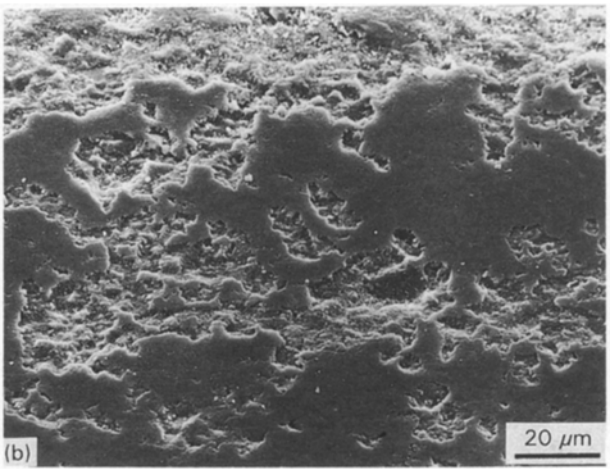

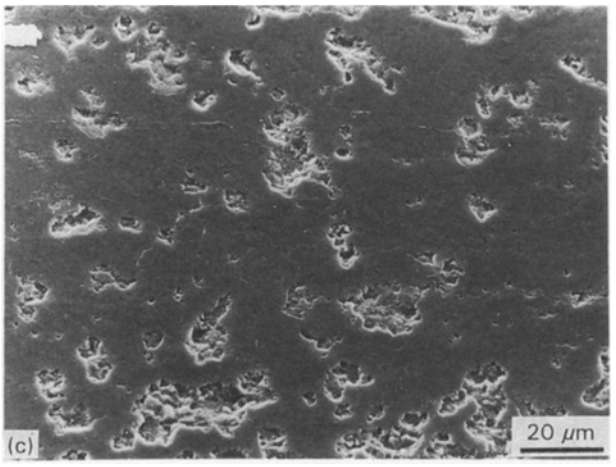

Figure 7 Surface of alumina after wear under loads of (a) 20 N, (b) 40 N and (c) 60 N.

minimizing macroscopic brittle fracture and improving wear resistance. Material removal in the equilibrium stage is mainly caused by plastic deformation and grain-boundary fracture. Wear resistance should thus be enhanced by increasing the hardness and grain-boundary fracture toughness. Recent work by Ajayi and Ludema [47] has shown that additions of silica, magnesia and calcia to alumina improve its wear resistance due to the formation of a glassy phase along the grain boundaries even though the hardness decreased. These results are consistent with the above mechanisms, because this amorphous phase is capable of viscous flow and is expected to improve the grain-boundary fracture toughness by accommodating the deformation of the neighbouring grains and reducing the residual stress levels.

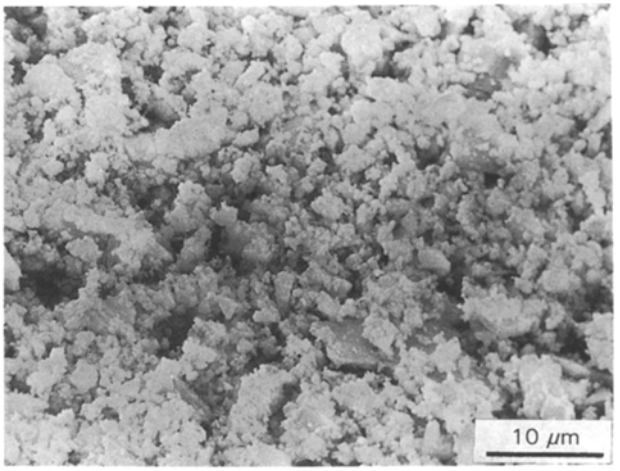

Figure 8 Debris resulting from the wear of alumina in the reciprocating diamond scratch test.

4. Conclusions

Several mechanical properties and wear behaviour of a well-characterized batch of as-sintered alumina specimens fabricated using injection moulding have been estimated in this investigation. The mechanical properties are: an average modulus of rupture of 268 MPa, a Weibull modulus of 7, an average hardness of 1540 kg mm^{-2} and an average K_{IC} value of 4.1 MPa $m^{1/2}$.

The main microstructural feature of failure during flexural testing was the linking together of micropores present in the test bars. Iron particles introduced to the alumina due to wear of processing machinery were also found on the fracture surfaces.

Wear under sliding took place in a severe running-in stage followed by a much milder equilibrium period. Wear during running-in was attributed to macroscopic brittle fracture and in the equilibrium stage, to plastic deformation and intergranular fracture. Material removal during equilibrium wear takes place by plastic deformation, the initiation of cracks at grain boundaries across the sliding direction, and their propagation around grain contours, resulting in grain pull-out.

Acknowledgements

The authors thank CNPq, Brazilian Government, for funding given to R. Nogueira. Technical support given by Mr K. K. Dutta and Mrs R. Pratt is acknowledged. Mrs K. Goddard is thanked for typing the manuscript.

References

1. A. G. EVANS, *J. Am. Ceram. Soc.* **65** (1982) 127.
2. H. SUZUKI. *Phil. Trans. R. Soc. Lond.* **A322** (1987) 465.
3. R. C. NEWHAM. *Proc. Br. Ceram. Soc.* **25** (1975) 281.
4. R. MORRELL. *Mater. Sci. Eng.* **A109** (1989) 131.
5. G. D. QUINN and R. MORRELL. *J. Am. Ceram. Soc.* **74** (1991) 2037.

6. C. F. LEWIS. *Mater. Eng.* **105** (1988) 41.
7. P. STANLEY. *Proc. Br. Ceram. Soc.* **39** (1987) 167.
8. B. BERGMAN. *J. Mater. Sci. Lett.* **3** (1984) 689.
9. *Idem. ibid.* **5** (1986) 611.
10. *Idem. Proc. Br. Ceram. Soc.* **39** (1987) 175.
11. D. J. CLINTON, I. A. LAY and R. MORRELL. *ibid.* **37** (1986) 217.
12. D. B. MARSHALL and B. R. LAWN, in, "Microindentation Techniques in Materials Science and Engineering", edited by P. J. Blau and B. R. Lawn (International Metallographic Society, Philadelphia, PA., 1986) pp. 26–46.
13. D. J. CLINTON and R. MORRELL. *Proc. Br. Ceram. Soc.* **34** (1984) 113.
14. R. MORRELL. "Handbook of Properties of Technical and Engineering Ceramics", Part I (HMSO, London, 1987).
15. C. B. PONTON and R. D. RAWLINGS. *Mater. Sci. Technol.* **5** (1989) 865.
16. C. F. LEWIS. *Mater. Eng.* **108** (1991) 31.
17. K. M. LIANG, G. ORANGE and G. FANTOZZI. *J. Mater. Sci.* **25** (1990) 207.
18. R. F. PABST, K. KROMP and G. POPP. *Proc. Br. Ceram. Soc.* **32** (1982) 89.
19. C. B. PONTON and R. D. RAWLINGS. *Mater. Sci. Technol.* **5** (1989) 961.
20. P. M. RAMSEY and T. F. PAGE. *Br. Ceram. Trans. J.* **87** (1988) 74.
21. J. F. BRAZA, H. S. CHENG, M. E. FINE, A. K. GANGOPADHYAY, L. M. KEER and R. E. WORDEN. *Tribol. Trans.* **32** (1989) 1.
22. S. M. HSU, Y. S. WANG and R. G. MUNRO. *Wear* **134** (1989) 1.
23. R. W. RICE. *Ceram. Eng. Sci. Proc.* **6** (1985) 940.
24. M. G. GEE. *Proc. Br. Ceram. Soc.* **46** (1990) 287.
25. K. E. AMIN. in "Engineered Materials Handbook", Vol. 4 (ASM International, Metals Park, Ohio, 1991), pp. 599–609.
26. P. M. RAMSEY and T. F. PAGE. *Br. Ceram. Trans. J.* **87** (1988) 74.
27. M. G. GEE and E. A. ALMOND. *Mater. Sci. Technol.* **4** (1988) 877.
28. A. J. PEREZ-UNZUETA, J. H. BEYNON and M. G. GEE. *Wear* **138** (1991) 179.
29. T. S. EYRE and F. A. DAVIS, in "Characterisation of High-Temperature Materials", Vol. 6, edited by T. N. Rhys-Jones (Institute of Metals, London, 1989) pp. 186–240.
30. D. T. GAWNE and U. MA. *Wear* **129** (1989) 123.
31. R. MORRELL. "Handbook of Properties of Technical and Engineering Ceramics", Part II (HMSO, London, 1987).
32. R. E. F. Q. NOGUEIRA, M. J. EDIRISINGHE and D. T. GAWNE. *J. Mater. Sci.* in press.
33. B. C. MUTSUDDY. *Powder Met. Int.* **19** (1987) 43.
34. A. J. FANELLI, R. D. SILVERS, W. S. FREI, J. V. BURLEW and G. B. MARSH. *J. Am. Ceram. Soc.* **72** (1989) 1833.
35. E. A. BARRINGER and H. K. BOWEN. *ibid* **65** (1982) C199.
36. H. P. KIRCHNER. "Strengthening of Ceramics" (Marcel Dekker, New York, 1977) p. 25.
37. R. G. HOAGLAND, C. W. MARSCHALL and W. H. DUCKWORTH. *J. Am. Ceram. Soc.* **59** (1975) 189.
38. N. BALAGOPAL, P. MUKUNDAN, K. G. K. WARRIER and A. D. DAMODARAN. *Br. Ceram. Trans. J.* **91** (1992) 80.
39. J. E. RITTER and R. W. DAVIDGE. *J. Am. Ceram. Soc.* **67** (1984) 432.
40. P. BOCH, J. C. GLANDUS and F. PLATON, in "2nd European Symposium on Engineering Ceramics", edited by F. L. Riley (Elsevier, London, UK, 1989) pp. 7–30.
41. B. G. NEWLAND. *ibid.* pp. 81–97.
42. J. C. GLANDUS and P. BOCH. *J. Mater. Sci. Lett.* **3** (1984) 74.
43. G. D. QUINN. *J. Am. Ceram. Soc.* **73** (1990) 2374.
44. M. G. GEE and E. A. ALMOND. *J. Mater. Sci.* **25** (1990) 296.
45. G. DONG, D. T. GAWNE and B. J. GRIFFITHS. in "Proceedings of the 3rd International Conference on Advances in Coatings and Surface Engineering", Newcastle, UK, May 1992, in press.
46. J. E. and D. T. GAWNE. to be published.
47. O. O. AJAYI and K. C. LUDEMA. *Wear* **154** (1992) 371.

Received 11 February
and accepted 24 February 1993